remote sensing

MDPI

Article

Evaluating the Differenced Normalized Burn Ratio for Assessing Fire Severity Using Sentinel-2 Imagery in Northeast Siberian Larch Forests

Clement J. F. Delcourt [1,*], Alisha Combee [1], Brian Izbicki [2], Michelle C. Mack [2], Trofim Maximov [3], Roman Petrov [3], Brendan M. Rogers [4], Rebecca C. Scholten [1], Tatiana A. Shestakova [4], Dave van Wees [1] and Sander Veraverbeke [1]

1 Faculty of Science, Vrije Universiteit Amsterdam, de Boelelaan 1085, 1081 HV Amsterdam, The Netherlands; a.combee@student.vu.nl (A.C.); r.c.scholten@vu.nl (R.C.S.); d.van.wees@vu.nl (D.v.W.); s.s.n.veraverbeke@vu.nl (S.V.)
2 Center for Ecosystem Science and Society, Northern Arizona University, Flagstaff, AZ 86011, USA; bi67@nau.edu (B.I.); Michelle.Mack@nau.edu (M.C.M.)
3 Institute for Biological Problems of Cryolithozone, Siberian Branch of the Russian Academy of Sciences, 41 Lenina Ave., Yakutsk 677000, Russia; tcmax@mail.ru (T.M.); pre2003@mail.ru (R.P.)
4 Woodwell Climate Research Center, Falmouth, MA 02540, USA; brogers@woodwellclimate.org (B.M.R.); tshestakova@woodwellclimate.org (T.A.S.)
* Correspondence: c.j.f.delcourt@vu.nl

check for updates

Citation: Delcourt, C.J.F.; Combee, A.; Izbicki, B.; Mack, M.C.; Maximov, T.; Petrov, R.; Rogers, B.M.; Scholten, R.C.; Shestakova, T.A.; van Wees, D.; et al. Evaluating the Differenced Normalized Burn Ratio for Assessing Fire Severity Using Sentinel-2 Imagery in Northeast Siberian Larch Forests. *Remote Sens.* **2021**, *13*, 2311. https://doi.org/10.3390/rs13122311

Academic Editor: Eldar Kurbanov

Received: 30 April 2021
Accepted: 9 June 2021
Published: 12 June 2021

Publisher's Note: MDPI stays neutral with regard to jurisdictional claims in published maps and institutional affiliations.

Copyright: © 2021 by the authors. Licensee MDPI, Basel, Switzerland. This article is an open access article distributed under the terms and conditions of the Creative Commons Attribution (CC BY) license (https://creativecommons.org/licenses/by/4.0/).

Abstract: Fire severity is a key fire regime characteristic with high ecological and carbon cycle relevance. Prior studies on boreal forest fires primarily focused on mapping severity in North American boreal forests. However, the dominant tree species and their impacts on fire regimes are different between North American and Siberian boreal forests. Here, we used Sentinel-2 satellite imagery to test the potential for using the most common spectral index for assessing fire severity, the differenced Normalized Burn Ratio (dNBR), over two fire scars and 37 field plots in Northeast Siberian larch-dominated (*Larix cajanderi*) forests. These field plots were sampled into two different forest types: (1) dense young stands and (2) open mature stands. For this evaluation, the dNBR was compared to field measurements of the Geometrically structured Composite Burn Index (GeoCBI) and burn depth. We found a linear relationship between dNBR and GeoCBI using data from all forest types ($R^2 = 0.42$, $p < 0.001$). The dNBR performed better to predict GeoCBI in open mature larch plots ($R^2 = 0.56$, $p < 0.001$). The GeoCBI provides a holistic field assessment of fire severity yet is dominated by the effect of fire on vegetation. No significant relationships were found between GeoCBI components (overall and substrate stratum) and burn depth within our fires ($p > 0.05$ in all cases). However, the dNBR showed some potential as a predictor for burn depth, especially in the dense larch forests ($R^2 = 0.63$, $p < 0.001$). In line with previous studies in boreal North America, the dNBR correlated reasonably well with field data of aboveground fire severity and showed some skills as a predictor of burn depth. More research is needed to refine spaceborne fire severity assessments in the larch forests of Northeast Siberia, including assessments of additional fire scars and integration of dNBR with other geospatial proxies of fire severity.

Keywords: fire severity; differenced normalized burn ratio; composite burn index; burn depth; Sentinel-2; Siberia; larch; boreal forest; remote sensing

1. Introduction

Wildfire is a natural disturbance that can drastically alter ecosystem composition, structure, function, and carbon stock [1,2]. Fires in boreal forests occur in remote and often inaccessible areas, burning large areas, and are of particular concern given the biome's large carbon stocks that are mostly contained in soil organic matter [3–6]. Therefore, remote sensing measurements are essential for quantifying the impact of fire in boreal forests, including the effect on ecological processes such as tree mortality, post-fire recovery, and carbon emissions [7]. Remotely sensed data provide powerful and cost-effective tools for mapping fire extents from local to global scales and assessing the degree of environmental changes caused by fire [8–10].

The environmental impact of wildfires in boreal regions differs from fires in other climate regions due to soil composition and climate conditions [7]. Boreal soils generally consist of a thick organic layer known as duff, which stores large amounts of carbon and acts as an insulating and protective layer for the underlying mineral soils and permafrost [11]. The organic carbon content builds up over time due to slow decomposition rates associated with cold temperatures and moist soil conditions [12]. This duff layer can be partially or completely consumed by fires and represents the majority of carbon emissions from boreal forest fires [13–15]. Previous studies showed that burn depths of 30 cm or more in organic soils can occur during severe fires [16–18], and as a result, the carbon combustion per unit area for boreal forests is among the largest on Earth [19]. Consumption of the duff layer and the vegetation can also lead to deepening of the active layer in areas with permafrost, which generates further carbon emissions due to higher fuel availability and, in some cases, complete permafrost degradation [20–22].

Climate change is intensifying boreal fire regimes by influencing the occurrence of lightning-ignited fires [4,23], fire size and regional burned area, and the timing of burning within the fire season [24]. Late season burning, for example, may lead to deeper burning in the soil organic layer because of drier fuel conditions and increased fuel availability within the seasonally thawed active layer [24]. These factors, together with gradients of soil moisture, influence the combustion of aboveground herbaceous and woody vegetation, belowground organic soils, and dead organic matter on the surface [24–26]. Because boreal fire frequency and burned area are increasing with climate change, carbon emissions from fires form an important positive feedback for climate warming [24,27,28]. Therefore, it is important to quantify the variability of boreal fire impacts within and across burns in order to better understand climate-fire feedbacks.

Fire severity usually refers to the immediate impacts of fire on the local environment and integrates post-fire measurements of the magnitude of fuel consumption (e.g., tree mortality, soil alteration, vegetation, and soil organic material consumption) [8,9]. The most commonly used field protocol for assessing fire severity is the Composite Burn Index (CBI) [8]. The CBI is a visual assessment tool to rapidly assess fire severity on a site. This index estimates the magnitude of fire effects for four different vegetation strata and the soil substrate and is therefore more strongly related to aboveground fire severity than belowground fire severity [8]. A modified version of the CBI, called the Geometrically structured CBI (GeoCBI), was proposed to take into account the influence of vegetation cover on reflectance of the different strata within a field site [29]. Field measurements are often combined with the Normalized Burn Ratio (NBR) [7,8,30–32], which is the most commonly used spectral index for assessing fire severity. This index combines near infrared (NIR) and short-wave infrared (SWIR) reflectance. As vegetation is consumed by fire, the NIR reflectance decreases, whereas the SWIR reflectance is relatively high due to the low moisture content of the burned areas [33]. Bi-temporal differencing of pre-fire and post-fire NBR images results in the differenced Normalized Burn Ratio (dNBR), which elucidates the fire-induced changes in NIR and SWIR reflectance [8]. The dNBR demonstrated skill as an indicator for aboveground severity due to its sensitivity to the decrease in vegetation greenness and landscape moisture content [7,34]. In addition, the dNBR can, to some extent, predict burn depth and belowground combustion [35]. Because burn depth strongly determines belowground combustion and influences post-fire regeneration, it is a commonly used proxy for fire severity in boreal forests [15,35]. The Siberian boreal forest covers approximately two thirds of the circumpolar boreal biome and is dominated by permafrost landscapes with large carbon stocks [36]. However, due to the inaccessible nature of these forests, very little research about forest fires has been conducted in this area, and the effects of these fires on the ecosystem remain poorly understood [37]. The majority of fire severity assessments have been conducted in boreal North America, mostly using Landsat imagery [7,31,32,34,38–41]. The most common tree species in boreal North America are black spruce (*Picea mariana*), white spruce (*Picea glauca*), jack pine (*Pinus banksiana*), lodgepole pine (*Pinus contorta*), aspen (*Populus* spp.), and birch (*Betula* spp.) [42]. Of these tree species, the majority of fires occur in black spruce stands [35]. Studies conducted in Alaska [34] and western Canada [39] found that spruce forests had the highest dNBR values on average, whereas deciduous forests had the lowest values. Overall, the results of prior studies that focused on the relationships between field and remotely sensed fire severity in boreal North America vary widely [7]. For example, some studies found strong linear relationships between CBI and dNBR when considering all vegetation types [34,39]. Other studies showed high correlations for specific vegetation types (R^2 ranged between 0.58 and 0.83) [34,43], whilst Epting et al. [31] and Hoy et al. [38] reported much lower correlations for others (R^2 ranged between 0.01 and 0.67). Non-linear models led to higher dNBR–CBI correlations [39,43–45]. Compared to boreal North America, fire regimes in Siberian boreal forests are substantially different due to the dominance of different tree species [46]. Siberian boreal forests are dominated by larch (*Larix* spp.) and Scots pine (*Pinus sylvestris*) species that cover approximately 50% and 20% of the forested areas in Siberia [47]. Satellite inferences showed that surface fires are more prevalent in larch forests in Siberia than in North American forest ecosystems [46]. These surface fires consume parts of the soil organic layer and the understory vegetation, yet the majority of trees survive due to their thick bark [48,49]. In the beginning of summer, surface fires can spread rapidly along the forest floor through the upper litter layer and the dead grass, resulting in low severity fires as the moisture content of most surface and ground fuels limits deep burning into the organic soils. Later in the season, or in dense stands with ladder fuels, surface fires can transition into high severity crown fires [47].

This study is the first, to our knowledge, to assess fire severity in Siberian larch ecosystems using a combination of field and satellite data. To do so, we derived dNBR from Sentinel-2 Multi-Spectral Instrument (MSI) imagery. The main objective of this paper is to evaluate the potential of dNBR derived from Sentinel-2 imagery as a proxy for fire severity in larch forest ecosystems in Northeast Siberia by evaluating its relationship with field data of fire severity.

2. Materials and Methods

2.1. Study Area

Our study sites in the Republic of Sakha (Russia) were located within two major fire events from 2017 and 2018 that burned approximately 800 and 910 km^2, respectively, near Batamay (63°31′N; 129°23′E) and Yert (62°01′N; 125°47′E) towns (Figure 1a). Most fires in Siberian boreal forests are considered to be surface fires, yet Rogers et al. [46] showed that Northeast Siberia experienced large areas of high severity stand-replacing fires in the last decades. We found evidence of surface and stand-replacing fire regimes in both fire scars. Lightning has been reported as the main cause of fires in high-latitude regions of Siberia [47]. Lightning ignitions occur especially during dry thunderstorms that are common during the summer months in Siberia. Dry conditions, strong winds, and evaporation of precipitation associated with these events create the conditions for rapid fire spread once ignited. In addition to lightning ignitions, human-caused ignitions occur near roads and settlements. Temperatures in Yakutsk vary between 18.7 °C (mean July temperature) and −42.6 °C (mean January temperature), and the mean annual precipitation rate is 234 mm [50]. Both sites lie in the zone of continuous permafrost, whose thickness varies widely within the Republic of Sakha, ranging from 70 to 1000 m [51]. Forests in both fire scars were characteristic of central Yakutia and largely dominated by a single larch species (i.e., *Larix cajanderi*) and with presence of Scots pine (*Pinus sylvestris*), silver birch (*Betula pendula*), alder species (*Alnus spp.*), and willow species (*Salix spp.*). Surface vegetation included cowberry (*Vaccinium vitis-idaea)*, bog blueberry (*Vaccinium uliginosum*), crowberry (*Empetrum nigrum*), rhododendron (*Rhododendron dauricum*), dog-rose (*Rosa acicularis*), spirea shrub (*Spiraea spp.*), juniper (*Juniperus spp.*), fireweed (*Epilobium angustifolium*), moss (e.g., *Ceratodon purpureus*, *Aulacomnium palustre*), and lichen. Composition, structure, and moisture content of these surface fuels influence fire characteristics and effects. For example, cowberry (*Vaccinium vitis-idaea*), one of the dominant shrub species within these forests, may act as a fire supporter, enhancing fire spread through fuels such as mosses, lichen, and litter [52].

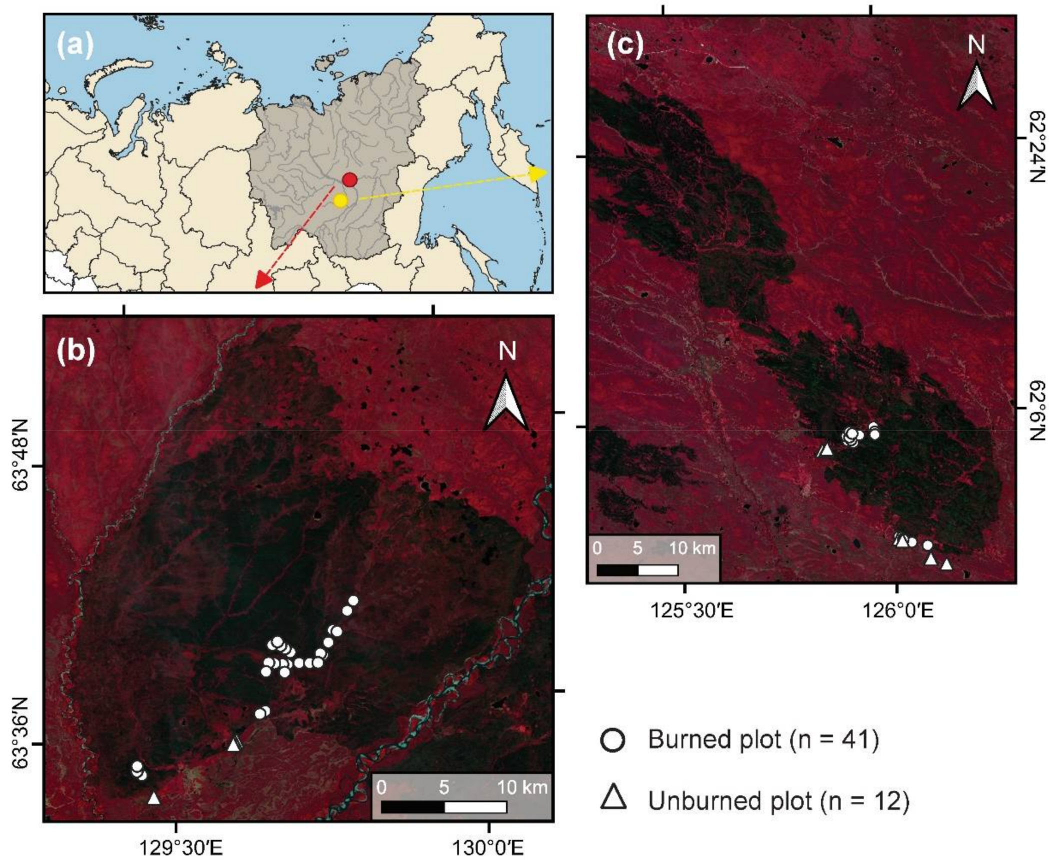

Figure 1. Study domain within the boreal forest of Northeast Siberia, Russia. (**a**) Fire scar locations in the Republic of Sakha (in brown), Russia (in yellow). The Batamay fire (red dot) burned between 25 June and 8 August 2017. The Yert fire (yellow dot) burned between 30 June and 21 July 2018. Sentinel-2 Multi Spectral Instrument (MSI) post-fire false color composites (level 2A, RGB–8A43) of (**b**) the Batamay fire (6 June 2018), and (**c**) the Yert fire (12 June 2019). White round markers depict the locations of burned plots, while triangular markers represent locations of unburned plots.

2.2. Field Data

Between 30 July and 22 August 2019, we sampled a total of 53 plots within both study sites, including 41 burned plots and 12 unburned plots (Figure 1b,c). We selected burned plots within a wide range of fire severity, vegetation composition, and landscape position based on geospatial data layers and visual assessment.

Each field plot was represented by a 30 m by 30 m quadrant which was selected within a relatively homogeneous and larger patch of vegetation and fire severity. Centroid coordinates and elevation were recorded using a high-precision GPS handheld device (GeoExplorer 7 series, Geo 7X, Trimble, 1 m horizontal and vertical accuracy). Geolocation of field plots was post-processed using information from the nearest reference station (Scripps Orbit and Permanent Array Center (SOPAC), Seismic Station Yakutsk, 62°01′51″N, 129°40′49″E, elevation: 103.41 m) providing decimeter accuracy. We also determined slope and aspect using a clinometer. Within each plot, we established a 30 m by 2 m belt transect in the north-south direction intersecting the plot's centroid using a similar design to Boby et al. [15], Rogers et al. [35], and Dieleman et al. [53]. Plots were allocated a moisture class, representing the potential moisture available for plant growth, according to a six-point scale, ranging from xeric to subhygric, as defined by Johnstone et al. [54]. This classification is primarily based on plot-level topographic drainage adjusted for soil texture and presence of permafrost. In the Yert fire scar, we also measured the active layer depth. Active layer depth was measured twice, with 1 m increments between both measurements, every 7.5 m along the belt transect, making for ten measurements per plot. Active layer depth was on average 127 cm (standard deviation: 27.8 cm) in burned plots and 98 cm (standard deviation: 26.9 cm) in unburned plots.

In burned plots, we investigated soil organic surface layers every 7.5 m along the transect (5 profiles per plot). For each soil profile, we measured the distance from the residual soil surface down to the A-horizon and the depth of the following organic horizons as defined by Manies et al. [55]: litter (dead plant materials such as leaves, bark, needles, and twigs), lichen, live moss, dead moss, fibric (slightly decomposed organic matter that contains more roots than recognizable moss parts), mesic (moderately decomposed material with few recognizable plant parts), and humic (highly decomposed material at the interface with the A-horizon with no identifiable plant parts). For sample points next to larch trees, we also recorded the distance between the residual SOL and the uppermost adventitious root on 1–2 roots per tree (Figure 2a). Adventitious roots are fine lateral roots that develop at shallower soil horizons as the trees grow in response to the dieback of their initial root system caused by colder and wetter conditions deeper in the soil column [56,57]. Adventitious roots remain visible on the bole of trees many years after the fire. Many studies showed that the position of these fine roots in the soil column can be used to estimate the height of the pre-fire soil surface and burn depth [15,17,35,58]. In addition, we measured total SOL depth and the distance from the top of the moss layer down to the highest adventitious root in unburned plots. We reconstructed pre-fire soil depth in burned plots based on a linear relationship between total SOL depth and the height of adventitious roots above the forest floor derived from these measurements in unburned plots (Figure 2b). The burn depth at each sample point was then estimated by subtracting the residual SOL depth from the retrieved pre-fire SOL depth. To account for the large heterogeneity in the consumption of duff observed in burned plots, we retrieved similar soil profiles at the base of ten additional trees randomly selected outside the belt transect within each plot. The final value for burn depth at the site-level was calculated as the average of (1) mean burn depth from its five soil cores and (2) burn depth calculated from the depth of burn at the ten trees.

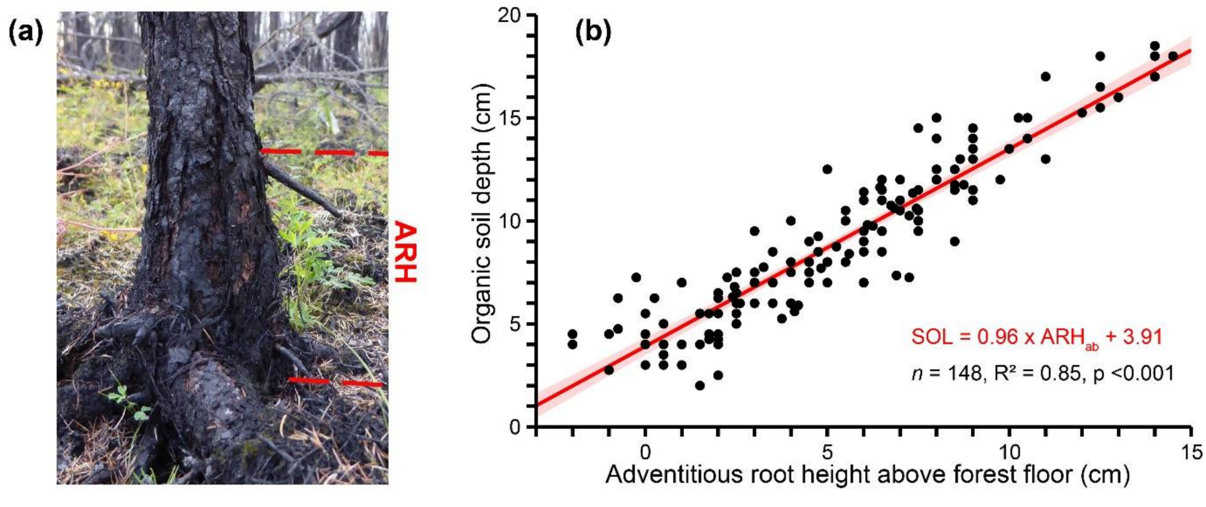

Figure 2. Adventitious root height (ARH) method used to retrieve pre-fire soil organic layer (SOL) depth in burned plots. (**a**) Picture showing adventitious roots on the bole of a burned tree. ARH is defined as the distance from the uppermost root to the residual soil surface. (**b**) Linear relationship between the pre-fire SOL and the ARH above forest floor (ARH_{ab} = ARH + residual SOL depth) derived from 148 paired SOL-ARH measurements in unburned plots.

In each plot, species and mortality status (i.e., alive, killed by the fire, dead before the fire and charred, and unknown) were recorded for every tree whose visible rooting system fell more than half within the belt transect. To estimate stand age, basal tree disks or cores were sampled from five trees of the dominant cohort.

In order to account for differences in vegetation structure and composition, we grouped our field plots in two forest types using a hierarchical clustering technique, called agglomerative clustering. In this bottom-up approach, each field plot was initially considered as an individual cluster. At each iteration, the pairs of clusters that minimally increased the linkage distance, a measure of dissimilarity between plots, were merged. This step was repeated until all plots were linked together in a hierarchical tree or dendrogram (Appendix A, Figure A1). Plot-level estimates of larch tree density, larch proportion, and stand age were standardized by subtracting mean values and dividing by the standard deviations (Table 1). Using these variables, we applied the Ward's method as linkage method in which the increase in total within-cluster sum of squared error was minimized [59,60]. In four burned plots and three unburned plots, we found mixed Cajander larch-Scots pine open forests where vegetation structure and soil properties differed from the larch-dominated plots. Due to their limited number and different characteristics, these plots were not included in this study. In total, 17 burned plots were assigned to dense, young-aged (50–70 years old) larch-dominated stands, and 20 burned plots were assigned to open, mature (110–130 years old) larch-dominated stands (Figure 3). Using the permafrost-landscape classification of Fedorov et al. [61], we estimated the spatial distribution of both forest types within Yert and Batamay fire scars as well as in the Republic of Sakha (Appendix B, Figure A2). All our field plots lie in the same vegetation unit that consists of larch forests characterized by low shrub and low shrub/lichen-moss covers. This vegetation landscape occupies 15.4% of total land area in the Republic of Sakha [61] and, respectively, 63.2% and 64.6% in Batamay and Yert fire scars.

Table 1. Descriptive statistics of forest structure and composition variables used in the hierarchical agglomerative clustering. LC: *Larix cajanderi*; LC prop.: larch trees proportion.

Descriptive Statistic	Dense Forest			Open Forest		
	LC Density (Trees m^{-2})	LC Prop. (0–1)	Stand Age (Years)	LC Density (Trees m^{-2})	LC Prop. (0–1)	Stand Age (Years)
n	17	17	17	20	20	20
Mean	2.00	0.80	55.30	0.55	0.65	112.00
Standard deviation	1.30	0.13	17.70	0.44	0.35	33.30
Minimum	0.63	0.51	9.00	0.07	0.09	63.00
Maximum	4.63	1.00	67.00	1.35	1.00	214.00

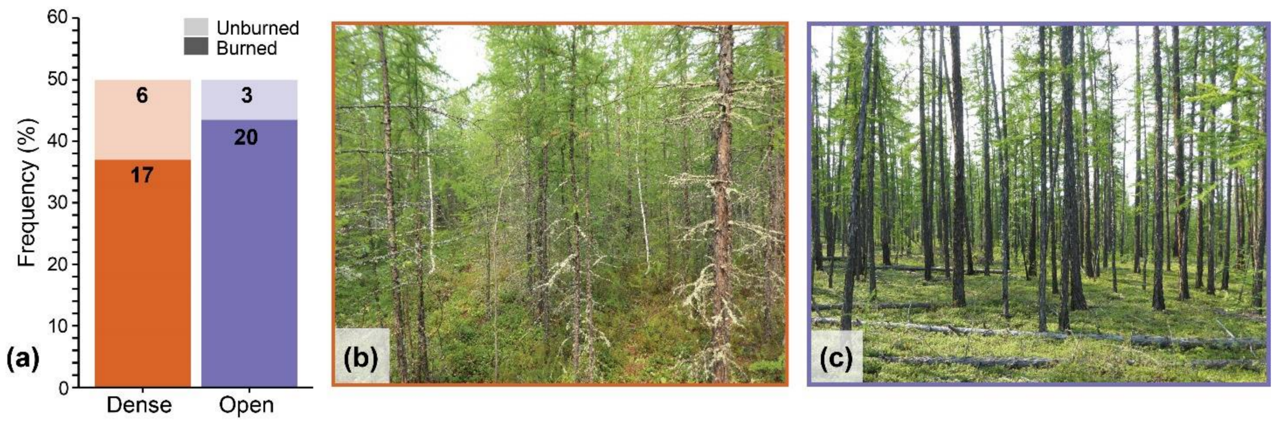

Figure 3. Forest types sampled within our study domain. (**a**) The actual number of burned and unburned plots in each forest type. Field pictures of typical unburned stands are shown for (**b**) dense, young aged larch-dominated (*Larix cajanderi*) forests, and (**c**) open mature larch-dominated forests.

Fire severity was visually assessed within each plot using the GeoCBI [29]. Through a continuous numeric scale ranging from 0 to 3, cumulative impacts of fire with respect to pre-fire conditions were gauged over the vertical structure of our forest stands (Figure 4). Using a hierarchical and multi-layered sampling design, the GeoCBI field protocol divides the plot into five different strata: (1) substrates (ground surface, litter, duff), (2) herbs, low shrubs, and trees less than 1 m, (3) tall shrubs and trees of 1 to 5 m, (4) intermediate trees of 5 to 20 m, and (5) trees higher than 20 m. Each stratum was divided into several subcategories which were evaluated independently using several criteria (e.g., percentage consumption of soil layers and vegetation, char height on the bole of trees, resprouting from burned vegetation (see Appendix C for the comprehensive list of criteria used in the field to compute the GeoCBI)). These subcategories were then assigned decimal values between 0 and 3, spanning the possible range of fire severity from no effect to high effect. The scores for each stratum were obtained by averaging the scores for all criteria and weighted by their fraction of coverage (FCOV) to compute the GeoCBI as follows:

$$\mathrm{GeoCBI} = \frac{\sum_{\mathrm{m_1}}^{\mathrm{m_n}} (\mathrm{CBI_m} \times \mathrm{FCOV_m})}{\sum_{\mathrm{m_1}}^{\mathrm{m_n}} \mathrm{FCOV_m}}, \quad (1)$$

where m refers to each individual stratum and n is the number of strata [29].

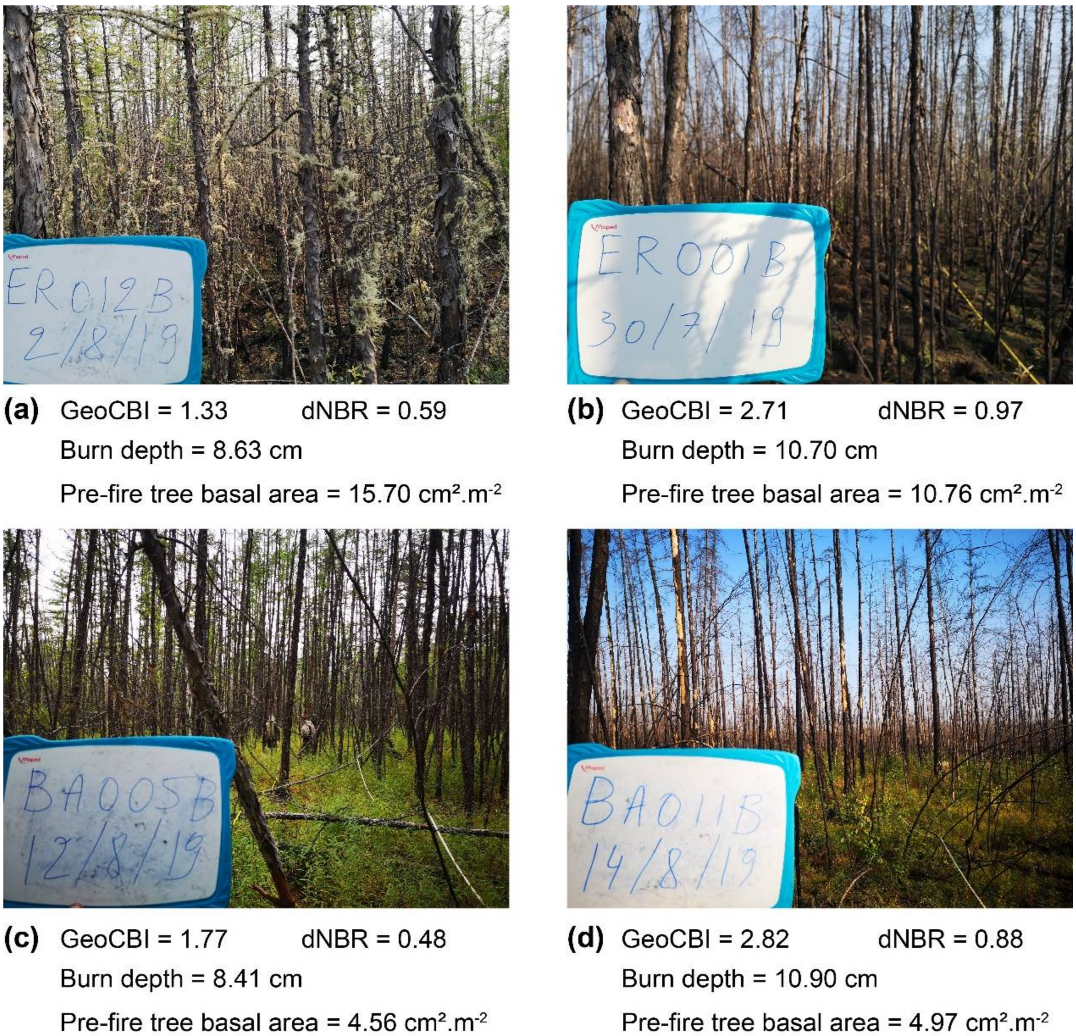

Figure 4. Field pictures depicting gradient of fire severity (from intermediate to high) in (**a**), (**b**) dense young larch-dominated forests, and in (**c**), (**d**) open mature larch-dominated forests. GeoCBI: Geometrically structured Composite Burn Index; dNBR: differenced Normalized Burn Ratio.

2.3. Imagery and Pre-Processing

Pre-fire and post-fire Sentinel-2 imagery processed to Level-1C were acquired from the Copernicus Open Access Hub website (https://scihub.copernicus.eu/, Table 2). For each scar, cloud-free pre-fire and post-fire scenes were selected at the beginning of the summer, respectively, one year prior to and one year after the fire event. Selecting images from the peak of the growing season, when unburned vegetation is green and lush, showed enhanced contrasts with burned areas [8]. Level-1C images were atmospherically corrected using the Sen2Cor Tool (version 2.8) [62] and converted to Level-2A Bottom-of-Atmosphere (BOA) reflectance (surface reflectance product). The Atmospheric Correction (AC) module of the Sen2Cor Tool is an adaptation of the Atmospheric and Topographic Correction (ATCOR) software [63] and includes the following parameters: (1) aerosol type (rural/continental or maritime), (2) atmosphere type (mid-latitude summer or mid-latitude winter), and (3) ozone content [62,64]. The last two parameters were configured according to the scenes' geographic location and climatology. A prerequisite for this was that all auxiliary data were present in the Level-1C input data [62]. Aerosol optical thickness (AOT) was derived at 550 nm based on the correlation between Sentinel-2 SWIR (B12), red (B4), and blue (B2) bands using the DDV (dense dark vegetation) algorithm [65]. To retrieve the water vapor column content, the Sen2Cor processor applied the Atmospheric Pre-corrected Differential Absorption algorithm [66] on Sentinel-2 bands B8A and B9. The rural aerosol type, the mid-latitude summer atmosphere, and an ozone content value of 331 DU (Dobson units) were used to correct each image for atmospheric effects. For the Yert fire, two separate tiles were mosaicked to cover the entire fire scar (Table 2). Pixel values in the overlapping area between the tiles were derived from the master image as part of the mosaicking procedure. No spectral disruptions between the images were visible after mosaicking.

Table 2. Summary attributes of Sentinel-2 image acquisition for both fire scars.

Fire Event	Data	Image Date	Row	Tile	Satellite
Batamay (2017)	Pre-fire	29/06/2016	32	T52VER	S2A
	Post-fire	09/06/2018	32	T52VER	S2A
Yert (2018)	Pre-fire	17/06/2017	75	T51VXJ	S2A
		17/06/2017	75	T51VXK	S2A
	Post-fire	12/06/2019	75	T51VXJ	S2B
		12/06/2019	75	T51VXK	S2B

The NBR was computed for each image using the 20 m resolution Sentinel-2 bands 8A (NIR) and 12 (SWIR) (Equation (2)), and dNBR was obtained from the temporal difference of NBR between pre-fire and post-fire scenes (Equation (3)) [8]. Although dNBR can theoretically vary between −2 and 2, values close to zero indicate unburned area and values close to 1 indicate severely burned area.

$$\mathrm{NBR} = \frac{\mathrm{NIR} - \mathrm{SWIR}}{\mathrm{NIR} + \mathrm{SWIR}} \quad (2)$$

$$\mathrm{dNBR} = \mathrm{NBR}_{\mathrm{pre-fire}} - \mathrm{NBR}_{\mathrm{post-fire}} \quad (3)$$

To correlate dNBR with GeoCBI and burn depth values sampled in the field, we averaged the index values within a 3×3 pixels window (60×60 m) centered around the plot locations. This approach minimized the effect of potential satellite misregistration [67].

2.4. Statistical Analysis

All data analyses were performed using R statistical software version 4.0.3 [68]. The cluster analysis was performed using the "agnes" function [69] from the R package "cluster" [70] with the dissimilarity metric and clustering method selected as "euclidean" and "ward". Prior to performing t-tests to evaluate differences in fire severity variables (GeoCBI, dNBR, burn depth) between forest types, we checked for the homogeneity of variances using Levene's test in the "car" package [71]. To investigate the relationships between the dNBR and the field data, we fitted linear regression models and derived a non-linear saturated growth model form using the R package "stats". For each regression model, we determined the coefficient of determination (R^2) and the root-mean-square-error (RMSE). We calculated three regression models for each relationship including (1) the dense young plots, (2) the open mature plots, and (3) the combined dataset. All statistical tests in this study were conducted at the 5% significance level.

3. Results

Differenced Normalized Burn Ratio (dNBR) maps of the two fire events around Yakutsk are shown in Figure 5. The spatial distribution of dNBR differed between the two fire scars. The Batamay fire showed a distinct pattern with a large core area of high dNBR values surrounded by areas of lower values. Of these areas, the western and the eastern parts of the scar experienced fires in 2001 and 2005, respectively (Appendix D, Figure A4). Only two plots were sampled in these previously burned areas. In the Yert fire scar, intermediate to high dNBR values were more homogeneously spread across the fire perimeter (Figure 5).

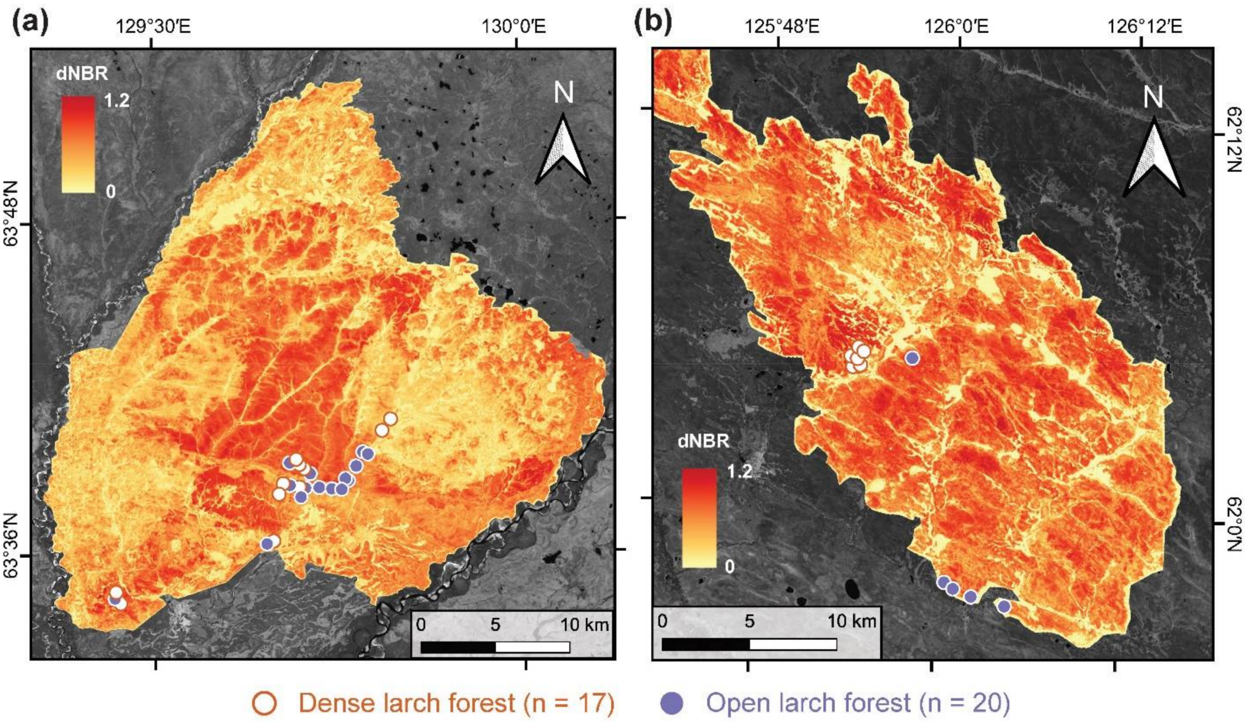

Figure 5. Differenced Normalized Burn Ratio (dNBR) maps of (**a**) the Batamay fire scar (2017) and (**b**) the Yert fire scar (2018). The colored dots represent the different forest types. The background images are post-fire Sentinel-2 SWIR band (B12) images.

Our field plots had dNBR values ranging between 0.19 and 1.06 (Table 3). Field-based and remotely sensed severity indices and their distribution were relatively similar across both forest types (GeoCBI: $p = 0.74$, dNBR: $p = 0.43$, two sample independent *t*-tests), with an average GeoCBI score of 2.49 for the dense larch dominated forests and 2.43 for the open forests (Figure 6, Table 3). However, a significant difference in burn depth was found between forest types ($p < 0.05$). Burn depth was, on average, 24.2% higher in open mature stands than in younger and more dense stands.

Table 3. Descriptive statistics of field and remotely sensed indices used to assess fire severity for each forest type. GeoCBI: Geometrically structured Composite Burn Index; dNBR: differenced Normalized Burn Ratio.

Descriptive Statistic	Dense Forest			Open Forest		
	GeoCBI	dNBR	Burn Depth (cm)	GeoCBI	dNBR	Burn Depth (cm)
n	17	17	17	20	20	20
Mean	2.49	0.69	8.00	2.43	0.63	9.94
Standard deviation	0.54	0.26	1.86	0.51	0.21	1.77
Minimum	1.33	0.19	4.06	1.53	0.24	6.68
Maximum	3.00	1.06	10.7	3.00	0.89	12.8

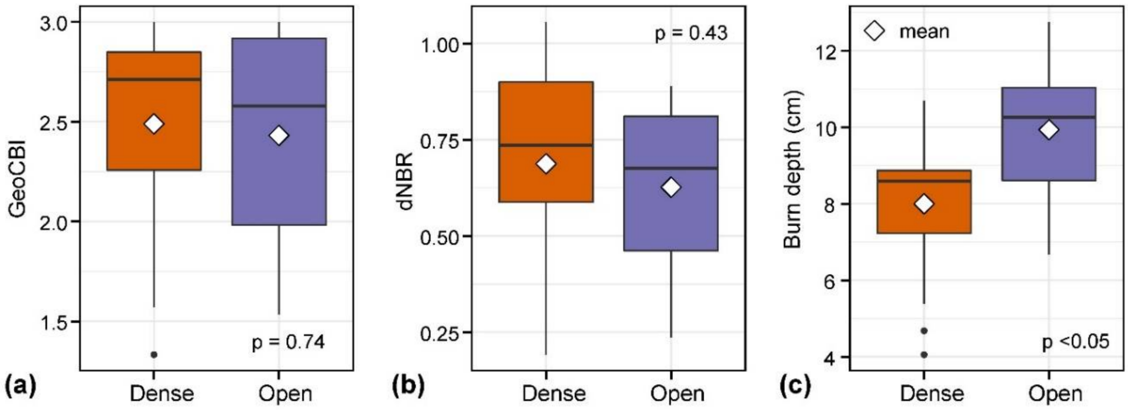

Figure 6. Field and remotely sensed fire severity indices in both forest types: (**a**) Geometrically structured Composite Burn Index (GeoCBI), (**b**) differenced Normalized Burn Ratio (dNBR), and (**c**) burn depth. Results of the two-sample independent t-tests performed to evaluate differences in mean values across forest types are indicated as p values. The horizontal black line within each box represents the median and the white dot indicates the mean.

To evaluate the potential of dNBR for assessing fire severity within our study area, we derived several regression models with field data as response variables (Figure 7 and Table 4). A significant linear correlation was found between GeoCBI and dNBR using data from all vegetation types ($R^2 = 0.42$, $p < 0.001$, Figure 7a). The correlation between GeoCBI and dNBR was still significant for study plots grouped by forest types ($p < 0.05$ for dense plots, $p < 0.001$ for open plots). The highest R^2 and the lowest RMSE were reported for the open forest type with values of 0.56 and 0.33, respectively (Table 4).

The relationship between dNBR and the substrate component of the GeoCBI was weaker when considering all strata (for all plots: $R^2 = 0.17$, $p < 0.05$, Figure 7b). No significant relationships were found for either of the two forest types ($p = 0.05$ for dense forests, $p = 0.15$ for open forests).

Neither the overall CBI nor the substrate CBI correlated strongly with burn depth (Figure 7c,d). This relationship was slightly stronger when only dense young plots were considered yet remained statistically insignificant (Table 4).

Lastly, the dNBR was tested as a predictor for burn depth using two regression model forms: (1) linear model (Figure 7e) and (2) non-linear model based on a saturated growth model form (Figure 7f). We found a weak linear relationship between dNBR and burn depth using all plots ($R^2 = 0.20$, $p < 0.05$). The saturated growth model performed slightly better with higher R^2 (0.22) and lower RMSE (1.77) values (Table 4). The strongest relationships for dNBR with burn depth were observed in dense young plots, while the regressions in open, more mature stands showed no relationships for both linear and saturated growth models (Figure 7e,f). The linear and the saturated growth regression models yielded similar performance for the dense young plots ($R^2 = 0.63$).

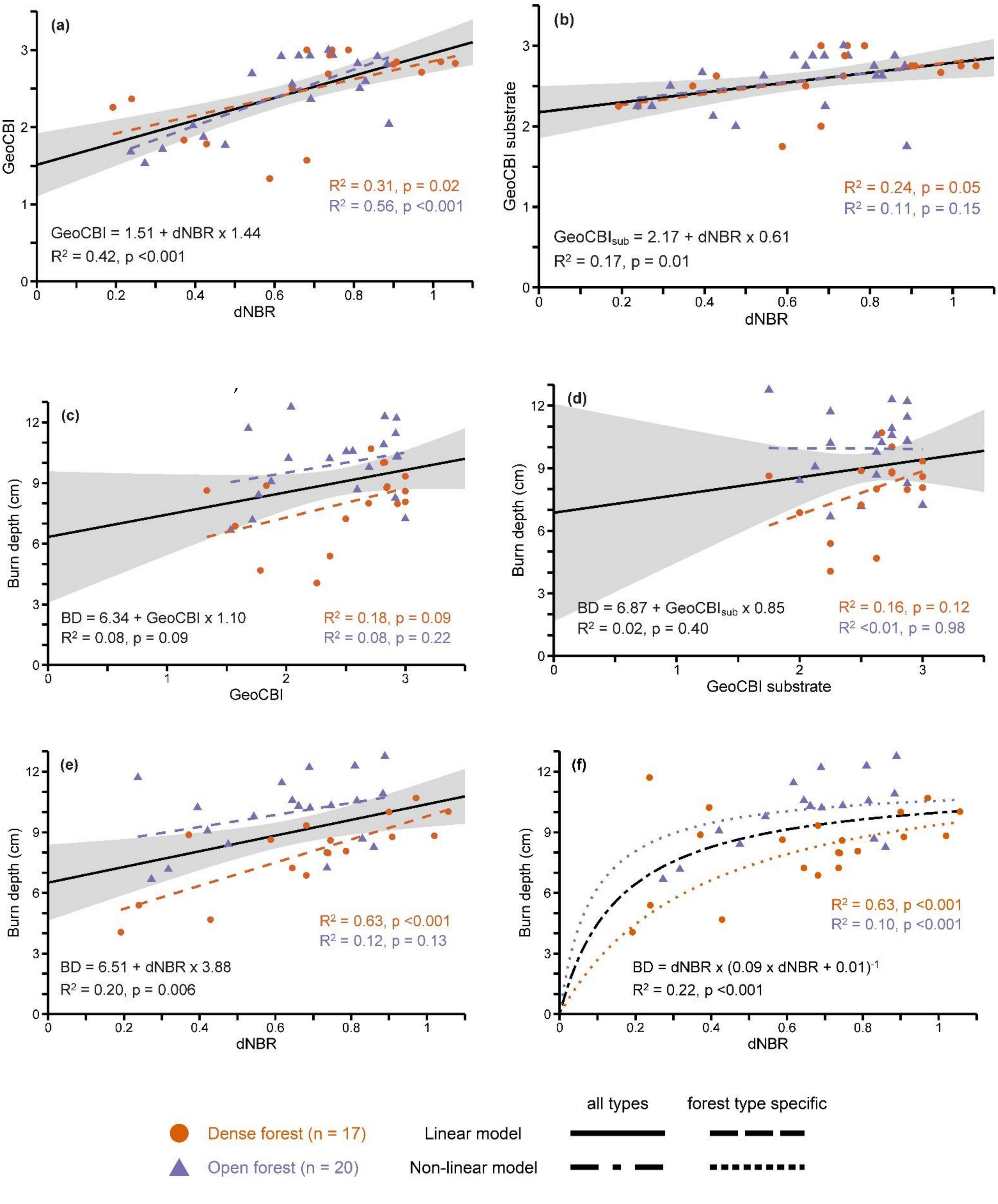

Figure 7. Scatterplots and model relationships between field and remotely sensed fire severity indices. (**a**) GeoCBI–dNBR; (**b**) $GeoCBI_{sub}$–dNBR; (**c**) BD–GeoCBI; (**d**) BD–$GeoCBI_{sub}$; (**e**) BD–dNBR, linear model; (**f**) BD–dNBR, non-linear model (saturation growth model form). GeoCBI: Geometrically structured Composite Burn Index; $GeoCBI_{sub}$: substrate component of the GeoCBI; dNBR: differenced Normalized Burn Ratio; BD: burn depth; R^2: coefficient of determination; RMSE: root mean square error. The shaded area indicates the 95% confidence interval. More results are summarized in Table 4.

Table 4. Linear and non-linear (saturated growth model form) modeling results for each forest type and the pooled dataset. GeoCBI: Geometrically structured Composite Burn Index; $GeoCBI_{sub}$: substrate component of the GeoCBI; dNBR: differenced Normalized Burn Ratio; BD: burn depth; R^2: coefficient of determination; RMSE: root mean square error. Each row of this table corresponds to a panel of Figure 7, indicated by small letters (a–f).

y–x	Dense Forest (n = 17)					Open Forest (n = 20)					Combined (n = 37)				
y = *a* + *b*(x)	**a**	**b**	**R^2**	**RMSE**	***p***	**a**	**b**	**R^2**	**RMSE**	***p***	**a**	**b**	**R^2**	**RMSE**	***p***
GeoCBI–dNBR[(a)]	1.69	1.17	0.31	0.44	0.02	1.29	1.81	0.56	0.33	<0.001	1.51	1.44	0.42	0.39	<0.001
$GeoCBI_{sub}$–dNBR[(b)]	2.13	0.67	0.24	0.30	0.05	2.22	0.55	0.11	0.32	0.15	2.17	0.61	0.17	0.31	0.01
BD–GeoCBI[(c)]	4.41	1.44	0.18	1.63	0.09	7.52	0.99	0.08	1.65	0.22	6.34	1.10	0.08	1.92	0.09
BD–$GeoCBI_{sub}$[(d)]	2.61	2.08	0.16	1.65	0.12	10.02	-0.03	<0.01	1.72	0.98	6.87	0.85	0.02	1.98	0.40
BD–dNBR[(e)]	4.06	5.73	0.63	1.09	<0.001	8.07	2.97	0.12	1.61	0.13	6.51	3.88	0.20	1.80	0.006
$y = x \times (a[x] + b)^{-1}$															
BD–dNBR[(f)]	0.08	0.03	0.63	1.09	<0.001	0.09	0.01	0.10	1.63	<0.001	0.09	0.01	0.22	1.77	<0.001

4. Discussion

This is the first study to use Sentinel-2 imagery for the assessment of fire severity in Siberia, where the majority of the global boreal forests are located. Sentinel-2's improved spatial resolution and radiometric accuracy enables higher fire severity classification accuracies and stronger relationships with field data of fire severity in Mediterranean forest and shrubland ecosystems [72,73]. The relatively short revisit time of five days of the Sentinel-2 constellation also increases the chances for acquiring cloud-free imagery compared to Landsat 8. Our study confirms the potential of Sentinel-2 imagery for fire severity assessments in boreal forests.

Despite the different dominant tree species and fire regimes, our results confirm earlier findings from studies in black spruce-dominated forests of North America. Our study shows that the dNBR is especially useful as a predictor of aboveground severity, as inferred from the relatively strong relationship between the dNBR and the GeoCBI [74]. To a lesser extent, the dNBR also demonstrated potential as a predictor of burn depth, which is a proxy of belowground fire severity. This finding corroborates earlier works that demonstrated statistically significant but not always strong relationships between the dNBR and the burn depth in black spruce forests of Alaska and Canada [32,35,40,74,75].

Another similarity to prior work is the saturation of the dNBR for high severity plots [7,34]. The dNBR clearly captures differences between low-to-moderate severity plots (e.g., GeoCBI values lower than 2) and high severity plots. However, in high severity plots with GeoCBI values higher than 2.5, the dNBR is not capable of discriminating between subtle differences (Figure 7a). This same rationale applies to the relationship with burn depth as response variable (Figure 7e). Considering these limitations, the dNBR may serve as a useful discriminator between the effects of surface and stand-replacing fire within fire perimeters. Nevertheless, ecosystem-specific characteristics such as drainage conditions, tree species composition, and tree density may confound the dNBR's ability to differentiate between subtle differences in high severity burning. This is also in agreement with ecosystem-specific relationships between the dNBR and the field measurements of severity derived in North American boreal forests. For example, Allen and Sorbel [34] found significant variation in the regression equations and the strength of the relationship between dNBR and CBI among vegetation community types.

In this study, discriminating between dense and open larch-dominated forest eco-systems improved predictive relationships in some cases compared to regressions that included data from all plots combined. For example, the linear regression model between dNBR and GeoCBI performed better for open mature plots. On the contrary, a strong correlation between dNBR and burn depth was found in dense young plots. A possible explanation for this could be that the post-fire images from dense forests capture more of the ground surface as a result of crown fires. In open forests, most fires are surface fires, leaving most of the tree foliage undamaged. This underlines the need for and the importance of sufficient field calibration of remotely sensed indices such as the dNBR for use as fire severity predictors. This is especially the case in ecosystems for which no prior field calibration has been conducted. More field calibrations are needed for Siberian larch ecosystems to make more accurate estimates of burn depth and fuel consumption from fires.

Some studies have questioned the effectiveness of unitless measure of fire severity such as CBI or GeoCBI for fire severity assessment in boreal forests [76]. We found that the overall GeoCBI was not correlated with the absolute depth of soil organic layers consumed by fire. The linear regression model investigating the relationship between the individual substrate component of the GeoCBI and the burn depth did not improve this relationship. Belowground fire severity (i.e., burn depth or organic layer consumption) is a particularly important characteristic of boreal fire regimes as the majority of boreal fire carbon emissions come from belowground carbon combustion [13–15]. To some degree, our findings support the idea of the dNBR's superiority as an indicator of aboveground fire severity (Figure 7a). However, our results also clearly show that the dNBR has potential as a predictor of belowground fire severity in larch ecosystems of Northeast Siberia, especially when considering differences in vegetation structure (Figure 7e,f). Aboveground and belowground severities are also partly correlated [35,74], which may explain the lower yet significant relationships that we observed between the dNBR and the burn depth for our dataset. The reduced performance of the dNBR as a predictor of burn depth also highlights that belowground fire severity and combustion cannot be derived solely from spectral data. The ground surface is often obscured by branches and foliage or located in the shadow of trees, influencing the reflectance of the organic soil surface acquired by satellites [7]. Synergistic use of the dNBR with information on landscape position, fuel type and density, and fire weather is necessary to further refine spatially explicit estimates of fire severity in larch-dominated forests. In addition, field calibration of the dNBR for fires in the extensive larch forest ecosystems of Northeast Siberia requires additional field measurements covering gradients of fuel types and fire severity. Such combinations are necessary since accurate and spatially resolved estimates of burn depth could significantly reduce uncertainties in carbon emissions estimates from Siberian forest fires.

5. Conclusions

This study evaluated the differenced Normalized Burn Ratio (dNBR) for assessing fire severity in larch forests of Northeast Siberia using Sentinel-2 imagery. Geometrically structured Composite Burn Index (GeoCBI) and burn depth into the organic soil were used as ground truth. The dNBR was a relatively strong predictor of the GeoCBI, a field measurement that assesses fire-induced ecosystem changes with larger weight to fire-induced vegetation changes than soil changes. The dNBR captured variability of low to high severity fires within burn scars but was unable to discriminate between subtle differences in high severity fires. We also found that the dNBR holds some predictive power for estimating burn depth in larch-dominated forests in Siberia. However, the burn depth–dNBR relationship was not sufficiently strong to warrant the stand-alone use of this index as burn depth predictor. The results confirmed that discriminating between vegetation types is important when assessing fire severity from spaceborne imagery. Tree density exhibited a clear influence on the performance of the relationships between field and remotely sensed fire severity proxies.

Our study is the first to assess the relationship between the remotely sensed dNBR and field measurements of fire severity over the larch-dominated forest of Northeast Siberia and calls for additional field calibration to cover different fuel types. These efforts are necessary steps towards the implementation of a spaceborne fire severity index for use in a regional fire emissions model for Northeast Siberia.

Author Contributions: Study design, S.V., C.J.F.D., and A.C.; field work preparation, C.J.F.D., T.M., and S.V.; field work, C.J.F.D., B.I., R.P., B.M.R., R.C.S., T.A.S., D.v.W., and S.V.; analysis, C.J.F.D. and A.C.; writing—original draft preparation, A.C. and C.J.F.D.; writing—review and editing, all authors; supervision, S.V.; funding acquisition, S.V. and B.M.R. All authors have read and agreed to the published version of the manuscript.

Funding: This research was funded by a Vidi grant for the project "Fires pushing trees North" (Grant # 016.Vidi.189.070) awarded to Sander Veraverbeke by the Dutch Research Council (NWO). Brendan M. Rogers acknowledges support from the Gordon and Betty Moore Foundation (Grant #8414).

Institutional Review Board Statement: Not applicable.

Informed Consent Statement: Not applicable.

Data Availability Statement: Publicly available datasets were analyzed in this study. This data can be found here: https://scihub.copernicus.eu/.

Conflicts of Interest: The authors declare no conflict of interest. The funders had no role in the design of the study; in the collection, analyses, or interpretation of data; in the writing of the manuscript, or in the decision to publish the results.

Appendix A. Hierarchical Agglomerative Clustering Results

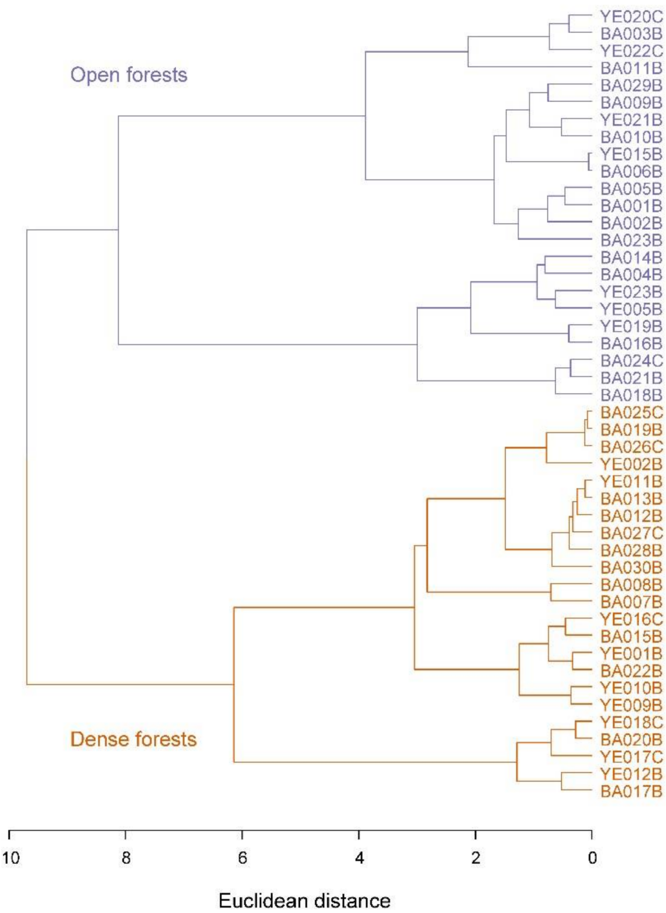

Figure A1. Dendrogram of the agglomerative clustering performed on the 46 field plots from both Batamay and Yert fire scars using larch (*Larix cajanderi*) density, larch proportion, and stand age data. In total, 23 plots were assigned to each forest type.

Appendix B. Spatial Distribution of Forest Types within Both Fire Scars

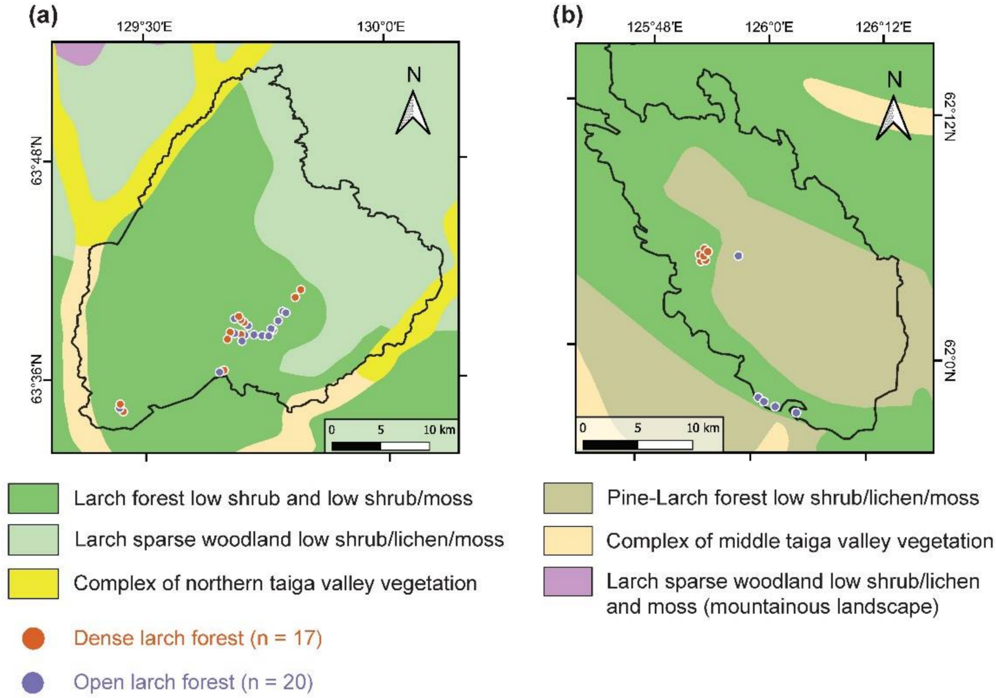

Figure A2. Spatial distribution of the larch-dominated forests within (**a**) Batamay and (**b**) Yert fire scars using the permafrost-landscape classification of Fedorov et al. [61].

Appendix C. Geometrically Structured Composite Burn Index Feld Protocol

STRATA	BURN SEVERITY SCALE							FACTOR SCORES
	No Effect	Low		Moderate		High		
	0	0.5	1.0	1.5	2.0	2.5	3.0	
A *SUBSTRATES*								
%DEAD LEAVES ON THE SOIL=						SOIL DEPTH (cm)=		
Litter/Light Fuel Consumed	Unchanged	--	50% litter	--	100% litter	>80% light fuel	98% light fuel	
Duff	Unchanged	--	light char	--	50% loss deep char	--	Consumed	
Medium /heavy Fuel	Unchanged	--	20% consumed	--	40% consumed	--	>60% loss, deep char	
Soil & Rock Cover/Color	Unchanged	--	10% change	--	40% change	--	>80% change	
			A. ∑ =		N=	$\bar{X}$=		
B *HERBS, LOW SHRUBS AND TREES LESS THAN 1 METER*								
DOMINANT VEGETATION TYPE =					FCOV=			
%Foliage altered (blk- brn)	Unchanged	--	30%	--	80%	95%	100%+branch loss	
Frequency % Living	100%	--	90%	--	50%	<20%	0%	
New sprouts	Abundant	--	moderate-high	--	moderate	--	low-none	
			B. ∑ =		N=	$\bar{X}$=		
C *TALL SHRUBS AND TREES 1 TO 5 METERS*								
DOMINANT VEGETATION TYPE =					FCOV=			
%Foliage altered (blk- brn)	0%	--	20%	--	60-90%	>95%	significant branch loss	
Frequency % Living	100%	--	90%	--	30%	<15%	<1%	
LAI change %	Unchanged	--	15%	--	70%	90%	100%	
			C. ∑ =		N=	$\bar{X}$=		
D *INTERMEDIATE TREES 5 TO 20 METERS*								
DOMINANT VEGETATION TYPE =					FCOV=			
% Green (unalterad)	100%	--	80%	--	40%	<10%	none	
%Black/ Brown	0%	--	20%	--	60-90%	>95%	significant branch loss	
Frequency % Living	100%	--	90%	--	30%	<15%	<1%	
LAI change %	Unchanged	--	15%	--	70%	90%	100%	
Char Height	none	--	1,5 m	--	2,8 m	--	>5 m	
			D. ∑ =		N=	$\bar{X}$=		
E *BIG TREES >20 METERS*								
DOMINANT VEGETATION TYPE =					FCOV=			
% Green (unalterad)	100%	--	95%	--	50%	<10%	none	
%Black/ Brown	0%	--	20%	--	60-90%	>95%	significant branch loss	
Frequency % Living	100%	--	90%	--	30%	<15%	<1%	
LAI change %	Unchanged	--	15%	--	70%	90%	100%	
Char Height	none	--	1,8 m	--	4 m	--	>7 m	
			E. ∑ =		N=	$\bar{X}$=		

Figure A3. The field form proposed by De Santis et al. [29] for estimating fire severity as Geometrically structured Composite Burn Index (GeoCBI).

Appendix D. Fire History within Batamay Area

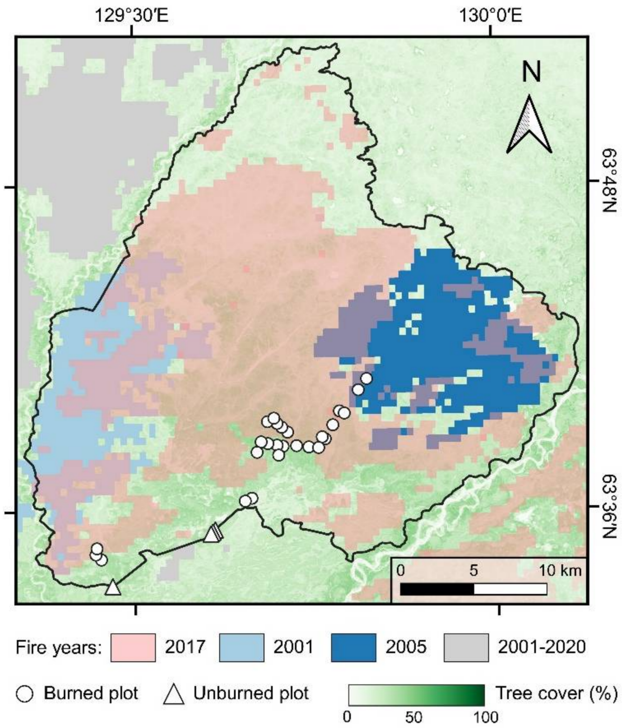

Figure A4. Map of the 2017 Batamay fire perimeter. Burned area data were derived from the Collection 6 MCD64A1 product [77]. Some areas within the scar experienced fires in 2001 and 2005. Two plots were sampled in these previously burned areas. The background image is the 30 m resolution tree cover product from the Global Forest Cover Change (GFCC30TC, v003) dataset for 2015 [78].

References

1. Harden, J.W.; Trumbore, S.E.; Stocks, B.J.; Hirsch, A.; Gower, S.T.; O'Neill, K.P.; Kasischke, E.S. The role of fire in the boreal carbon budget. *Glob. Chang. Biol.* **2000**, *6*, 174–184. [CrossRef]
2. Flannigan, M.D.; Stocks, B.J.; Wotton, B.M. Climate change and forest fires. *Sci. Total Environ.* **2000**, *262*, 221–229. [CrossRef]
3. Walker, X.J.; Baltzer, J.L.; Cumming, S.G.; Day, N.J.; Ebert, C.; Goetz, S.; Johnstone, J.F.; Potter, S.; Rogers, B.M.; Schuur, E.A.G.; et al. Increasing wildfires threaten historic carbon sink of boreal forest soils. *Nature* **2019**, *572*, 520–523. [CrossRef]
4. Veraverbeke, S.; Rogers, B.M.; Goulden, M.L.; Jandt, R.R.; Miller, C.E.; Wiggins, E.B.; Randerson, J.T. Lightning as a major driver of recent large fire years in North American boreal forests. *Nat. Clim. Chang.* **2017**, *7*, 529–534. [CrossRef]
5. Bradshaw, C.J.A.; Warkentin, I.G. Global estimates of boreal forest carbon stocks and flux. *Glob. Planet. Change* **2015**, *128*, 24–30. [CrossRef]
6. Flannigan, M.; Stocks, B.; Turetsky, M.; Wotton, M. Impacts of climate change on fire activity and fire management in the circumboreal forest. *Glob. Chang. Biol.* **2009**, *15*, 549–560. [CrossRef]
7. French, N.H.F.; Kasischke, E.S.; Hall, R.J.; Murphy, K.A.; Verbyla, D.L.; Hoy, E.E.; Allen, J.L. Using Landsat data to assess fire and burn severity in the North American boreal forest region: An overview and summary of results. *Int. J. Wildl. Fire* **2008**, *17*, 443–462. [CrossRef]
8. Key, C.H.; Benson, N.C. Landscape assessment (LA): Sampling and analysis methods. In *FIREMON: Fire Effects Monitoring and Inventory System*; Gen. Tech. Rep. RMRS-GTR-164; Lutes, D.C., Keane, R.E., Caratti, J.F., Key, C.H., Benson, N.C., Sutherland, S., Gangi, L.J., Eds.; USDA Forest Service, Rocky Mountain Research Station: Ogden, UT, USA, 2005.
9. Lentile, L.B.; Holden, Z.A.; Smith, A.M.S.; Falkowski, M.J.; Hudak, A.T.; Morgan, P.; Lewis, S.A.; Gessler, P.E.; Benson, N.C. Remote sensing techniques to assess active fire characteristics and post-fire effects. *Int. J. Wildl. Fire* **2006**, *15*, 319–345. [CrossRef]
10. De Santis, A.; Chuvieco, E. Burn Severity Estimation from Remotely Sensed Data: Performance of Simulation versus Empirical Models. *Remote Sens. Environ.* **2007**, *108*, 422–435. [CrossRef]
11. Gorham, E. Northern Peatlands: Role in the Carbon Cycle and Probable Responses to Climatic Warming. *Ecol. Appl.* **1991**, *1*, 182–195. [CrossRef]
12. Hobbie, S.E.; Schimel, J.P.; Trumbore, S.E.; Randerson, J.R. Controls over carbon storage and turnover in high-latitude soils. *Glob. Chang. Biol.* **2000**, *6*, 196–210. [CrossRef]

13. Kasischke, E.S.; Christensen, N.L., Jr.; Stocks, B.J. Fire, Global Warming, and the Carbon Balance of Boreal Forests. *Ecol. Appl.* **1995**, *5*, 437–451. [CrossRef]
14. Amiro, B.D.; Stocks, B.J.; Alexander, M.E.; Flannigan, M.D.; Wotton, B.M. Fire, climate change, carbon and fuel management in the Canadian boreal forest. *Int. J. Wildl. Fire* **2001**, *10*, 405–413. [CrossRef]
15. Boby, L.A.; Schuur, E.A.G.; Mack, M.C.; Verbyla, D.; Johnstone, J.F. Quantifying fire severity, carbon, and nitrogen emissions in Alaska's boreal forest. *Ecol. Appl.* **2010**, *20*, 1633–1647. [CrossRef]
16. Miyanishi, K.; Johnson, E.A. Process and patterns of duff consumption in the mixedwood boreal forest. *Can. J. For. Res.* **2002**, *32*, 1285–1295. [CrossRef]
17. Kasischke, E.S.; Johnstone, J.F. Variation in postfire organic layer thickness in a black spruce forest complex in interior Alaska and its effects on soil temperature and moisture. *Can. J. For. Res.* **2005**, *35*, 2164–2177. [CrossRef]
18. Harden, J.W.; Manies, K.L.; Turetsky, M.R.; Neff, J.C. Effects of wildfire and permafrost on soil organic matter and soil climate in interior Alaska. *Glob. Chang. Biol.* **2006**, *12*, 2391–2403. [CrossRef]
19. van Leeuwen, T.T.; van Der Werf, G.R.; Hoffmann, A.A.; Detmers, R.G.; Rücker, G.; French, N.H.F.; Archibald, S.; Carvalho, J.A.; Cook, G.D.; De Groot, W.J.; et al. Biomass Burning Fuel Consumption Rates: A Field Measurement Database. *Biogeosciences* **2014**, *11*, 7305–7329. [CrossRef]
20. Swanson, D.K. Susceptibility of permafrost soils to deep thaw after forest fires in interior Alaska, U.S.A., and some ecologic implications. *Arct. Alp. Res.* **1996**, *28*, 217–227. [CrossRef]
21. Jafarov, E.E.; Romanovsky, V.E.; Genet, H.; McGuire, A.D.; Marchenko, S.S. The effects of fire on the thermal stability of permafrost in lowland and upland black spruce forests of interior Alaska in a changing climate. *Environ. Res. Lett.* **2013**, *8*. [CrossRef]
22. Minsley, B.J.; Pastick, N.J.; Wylie, B.K.; Brown, D.R.N.; Kass, M.A. Evidence for nonuniform permafrost degradation after fire in boreal landscapes. *J. Geophys. Res. Earth Surf.* **2016**, *121*, 320–335. [CrossRef]
23. Kasischke, E.S.; Verbyla, D.L.; Rupp, T.S.; McGuire, A.D.; Murphy, K.A.; Jandt, R.; Barnes, J.L.; Hoy, E.E.; Duffy, P.A.; Calef, M.; et al. Alaska's changing fire regime—Implications for the vulnerability of its boreal forests. *Can. J. For. Res.* **2010**, *40*, 1360–1370.
24. Turetsky, M.R.; Kane, E.S.; Harden, J.W.; Ottmar, R.D.; Manies, K.L.; Hoy, E.; Kasischke, E.S. Recent acceleration of biomass burning and carbon losses in Alaskan forests and peatlands. *Nat. Geosci.* **2010**, *4*, 27–31. [CrossRef]
25. Walker, X.J.; Rogers, B.M.; Baltzer, J.L.; Cumming, S.G.; Day, N.J.; Goetz, S.J.; Johnstone, J.F.; Schuur, E.A.G.; Turetsky, M.R.; Mack, M.C. Cross-scale controls on carbon emissions from boreal forest megafires. *Glob. Chang. Biol.* **2018**, *24*, 4251–4265. [CrossRef] [PubMed]
26. Walker, X.J.; Rogers, B.M.; Veraverbeke, S.; Johnstone, J.F.; Baltzer, J.L.; Barrett, K.; Bourgeau-Chavez, L.; Day, N.J.; de Groot, W.J.; Dieleman, C.M.; et al. Fuel availability not fire weather controls boreal wildfire severity and carbon emissions. *Nat. Clim. Chang.* **2020**. [CrossRef]
27. Ponomarev, E.I.; Kharuk, V.I.; Ranson, K.J. Wildfires dynamics in Siberian larch forests. *Forests* **2016**, *7*, 125. [CrossRef]
28. Hanes, C.C.; Wang, X.; Jain, P.; Parisien, M.-A.; Little, J.M.; Flannigan, M.D. Fire-regime changes in Canada over the last half century. *Can. J. For. Res.* **2019**, *49*, 256–269. [CrossRef]
29. De Santis, A.; Chuvieco, E. GeoCBI: A modified version of the Composite Burn Index for the initial assessment of the short-term burn severity from remotely sensed data. *Remote Sens. Environ.* **2009**, *113*, 554–562. [CrossRef]
30. López García, M.J.; Caselles, V. Mapping burns and natural reforestation using thematic Mapper data. *Geocarto Int.* **1991**, *6*, 31–37. [CrossRef]
31. Epting, J.; Verbyla, D.; Sorbel, B. Evaluation of remotely sensed indices for assessing burn severity in interior Alaska using Landsat TM and ETM+. *Remote Sens. Environ.* **2005**, *96*, 328–339. [CrossRef]
32. Verbyla, D.; Lord, R. Estimating post-fire organic soil depth in the Alaskan boreal forest using the Normalized Burn Ratio. *Int. J. Remote Sens.* **2008**, *29*, 3845–3853. [CrossRef]
33. Key, C.H. Ecological and Sampling Constraints on Defining Landscape Fire Severity. *Fire Ecol.* **2006**, *2*, 34–59. [CrossRef]
34. Allen, J.L.; Sorbel, B. Assessing the differenced Normalized Burn Ratio's ability to map burn severity in the boreal forest and tundra ecosystems of Alaska's national parks. *Int. J. Wildl. Fire* **2008**, *17*, 463–475. [CrossRef]
35. Rogers, B.M.; Veraverbeke, S.; Azzari, G.; Czimczik, C.I.; Holden, S.R.; Mouteva, G.O.; Sedano, F.; Treseder, K.K.; Randerson, J.T. Quantifying Fire-Wide Carbon Emissions in Interior Alaska Using Field Measurements and Landsat Imagery. *J. Geophys. Res. Biogeosci.* **2014**, *119*, 1608–1629. [CrossRef]
36. Hare, F.K.; Ritchie, J.C. The Boreal Bioclimates. *Geogr. Rev.* **1972**, *62*, 333–365. [CrossRef]
37. Veraverbeke, S.; Delcourt, C.J.F.; Kukavskaya, E.; Mack, M.; Walker, X.; Hessilt, T.; Rogers, B.; Scholten, R.C. Direct and longer-term carbon emissions from arctic-boreal fires: A short review of recent advances. *Curr. Opin. Environ. Sci. Health* **2021**. [CrossRef]
38. Hoy, E.E.; French, N.H.F.; Turetsky, M.R.; Trigg, S.N.; Kasischke, E.S. Evaluating the potential of Landsat TM/ETM+ imagery for assessing fire severity in Alaskan black spruce forests. *Int. J. Wildl. Fire* **2008**, *17*, 500–514. [CrossRef]
39. Hall, R.J.; Freeburn, J.T.; de Groot, W.J.; Pritchard, J.M.; Lynham, T.J.; Landry, R. Remote sensing of burn severity: Experience from western Canada boreal fires. *Int. J. Wildl. Fire* **2008**, *17*, 476–489. [CrossRef]
40. Barrett, K.; Kasischke, E.S.; McGuire, A.D.; Turetsky, M.R.; Kane, E.S. Modeling fire severity in black spruce stands in the Alaskan boreal forest using spectral and non-spectral geospatial data. *Remote Sens. Environ.* **2010**, *114*, 1494–1503. [CrossRef]

41. Murphy, K.A.; Reynolds, J.H.; Koltun, J.M. Evaluating the ability of the differenced Normalized Burn Ratio (dNBR) to predict ecologically significant burn severity in Alaskan boreal forests. *Int. J. Wildl. Fire* **2008**, *17*, 490–499. [CrossRef]
42. Johnson, E.A. *Fire and Vegetation Dynamics: Studies from the North American Boreal Forest*; Cambridge University Press: Cambridge, UK, 1992; ISBN 978-051-162-351-6.
43. Zhu, Z.; Key, C.; Ohlen, D.; Benson, N. *Evaluate Sensitivities of Burn Severity Mapping Algorithms for Different Ecosystems and Fire Histories in the United States*; Final Report to the Joint Fire Science Program, Project JFSP 01–1-4–12; USGS, National Center for Earth Resources Observation and Science: Sioux Falls, SD, USA, 2006.
44. van Wagtendonk, J.W.; Root, R.R.; Key, C.H. Comparison of AVIRIS and Landsat ETM+ detection capabilities for burn severity. *Remote Sens. Environ.* **2004**, *92*, 397–408. [CrossRef]
45. Miller, J.D.; Thode, A.E. Quantifying burn severity in a heterogeneous landscape with a relative version of the delta Normalized Burn Ratio (dNBR). *Remote Sens. Environ.* **2007**, *109*, 66–80. [CrossRef]
46. Rogers, B.M.; Soja, A.J.; Goulden, M.L.; Randerson, J.T. Influence of tree species on continental differences in boreal fires and climate feedbacks. *Nat. Geosci.* **2015**, *8*, 228–234. [CrossRef]
47. Kharuk, V.I.; Ponomarev, E.I.; Ivanova, G.A.; Dvinskaya, M.L.; Coogan, S.C.P.; Flannigan, M.D. Wildfires in the Siberian taiga. *Ambio* **2021**. [CrossRef] [PubMed]
48. Nikolov, N.; Helmisaari, H. Silvics of the circumpolar boreal forest tree species. In *A Systems Analysis of the Global Boreal Forest*; Shugart, H.H., Leemans, R., Bonan, G.B., Eds.; Cambridge University Press: Cambridge, UK, 1992; pp. 13–84. ISBN 978-051-156-548-9.
49. Richardson, D.M.; Rundel, P.W. Ecology and biogeography of Pinus: An introduction. In *Ecology and Biogeography of Pinus*; Richardson, D.M., Ed.; Cambridge University Press: New-York, USA, 1998; pp. 3–46. ISBN 978-052-155-176-2.
50. Fedorov, A.N.; Konstantinov, P.Y.; Vasilyev, N.F.; Shestakova, A.A. The influence of boreal forest dynamics on the current state of permafrost in Central Yakutia. *Polar Sci.* **2019**, *22*. [CrossRef]
51. Zyryanova, O.A.; Abaimov, A.P.; Bugaenko, T.N.; Bugaenko, N.N. Recovery of Forest Vegetation After Fire Disturbance. In *Permafrost Ecosystems*; Osawa, A., Zyryanova, O.A., Matsuura, Y., Kajimoto, T., Wein, R.W., Eds.; Springer Netherlands: Dordrecht, The Netherlands, 2010; Volume 209, pp. 83–96. ISBN 978-1-4020-9692-1.
52. Ivanova, G.A.; Kukavskaya, E.A.; Ivanov, V.A.; Conard, S.G.; McRae, D.J. Fuel Characteristics, loads and consumption in Scots pine forests of central Siberia. *J. For. Res.* **2020**, *31*, 2507–2524. [CrossRef]
53. Dieleman, C.M.; Rogers, B.M.; Potter, S.; Veraverbeke, S.; Johnstone, J.F.; Laflamme, J.; Solvik, K.; Walker, X.J.; Mack, M.C.; Turetsky, M.R. Wildfire combustion and carbon stocks in the southern Canadian boreal forest: Implications for a warming world. *Glob. Chang. Biol.* **2020**, *26*, 6062–6079. [CrossRef] [PubMed]
54. Johnstone, J.F.; Hollingsworth, T.N.; Chapin, F.S. *A Key Predicting Postfire Successional Trajectories in Black Spruce Stands of Interior Alaska*; General Technical Report No. PNW-GTR-767; U.S. Department of Agriculture, Forest Service, Pacific Northwest Research Station: Portland, OR, USA, 2008.
55. Manies, K.L.; Harden, J.W.; Silva, S.R.; Briggs, P.H.; Schmid, B.M. *Soil Data from Picea mariana Stands near Delta Junction, Alaska of Different Ages and Soil Drainage Type*; Open-File Report 2004-1271; U.S. Department of the Interior, U.S. Geological Survey: Anchorage, AK, USA, 2004. Available online: https://pubs.usgs.gov/of/2004/1271/ (accessed on 6 April 2021).
56. Kajimoto, T.; Matsuura, Y.; Osawa, A.; Prokushkin, A.S.; Sofronov, M.A.; Abaimov, A.P. Root system development of *Larix gmelinii* trees affected by micro-scale conditions of permafrost soils in central Siberia. *Plant Soil* **2003**, *255*, 281–292. [CrossRef]
57. Kajimoto, T. Root System Development of Larch Trees Growing on Siberian Permafrost. In *Permafrost Ecosystems*; Osawa, A., Zyryanova, O.A., Matsuura, Y., Kajimoto, T., Wein, R.W., Eds.; Springer Netherlands: Dordrecht, The Netherlands, 2010; Volume 209, pp. 303–330. ISBN 978-1-4020-9692-1.
58. Walker, X.J.; Baltzer, J.L.; Cumming, S.G.; Day, N.J.; Johnstone, J.F.; Rogers, B.M.; Solvik, K.; Turetsky, M.R.; Mack, M.C. Soil organic layer combustion in boreal black spruce and jack pine stands of the Northwest Territories, Canada. *Int. J. Wildl. Fire* **2018**, *27*, 125–134. [CrossRef]
59. Ward, J.H., Jr. Hierarchical Grouping to Optimize an Objective Function. *J. Am. Stat. Assoc.* **1963**, *58*, 236–244. [CrossRef]
60. Szekely, G.J.; Rizzo, M.L. Hierarchical Clustering via Joint Between-Within Distances: Extending Ward's Minimum Variance Method. *J. Classif.* **2005**, *22*, 151–183. [CrossRef]
61. Fedorov, A.N.; Vasilyev, N.F.; Torgovkin, Y.I.; Shestakova, A.A.; Varlamov, S.P.; Zheleznyak, M.N.; Shepelev, V.V.; Konstantinov, P.Y.; Kalinicheva, S.S.; Basharin, N.I.; et al. Permafrost-Landscape Map of the Republic of Sakha (Yakutia) on a Scale 1:1,500,000. *Geosciences* **2018**, *8*, 465. [CrossRef]
62. Main-Knorn, M.; Pflug, B.; Louis, J.; Debaecker, V.; Müller-Wilm, U.; Gascon, F. Sen2Cor for Sentinel-2. In *Image and Signal Processing for Remote Sensing XXIII, Proceedings of the Society of Photo-Optical Instrumentation Engineers Remote Sensing, Warsaw, Poland, 4 October 2017*; International Society for Optics and Photonics: Bellingham, WA, USA; Volume 10427. [CrossRef]
63. Richter, R.; Schläpfer, D.; Müller, A. An automatic atmospheric correction algorithm for visible/NIR imagery. *Int. J. Remote Sens.* **2006**, *27*, 2077–2085. [CrossRef]
64. Mayer, B.; Kylling, A. Technical note: The libRadtran software package for radiative transfer calculations-description and examples of use. *Atmos. Chem. Phys.* **2005**, *5*, 1855–1877. [CrossRef]
65. Kaufman, Y.J.; Sendra, C. Algorithm for automatic atmospheric corrections to visible and near-IR satellite imagery. *Int. J. Remote Sens.* **1988**, *9*, 1357–1381. [CrossRef]

66. Schläpfer, D.; Borel, C.C.; Keller, J.; Itten, K.I. Atmospheric Precorrected Differential Absorption Technique to Retrieve Columnar Water Vapor. *Remote Sens. Environ.* **1998**, *65*, 353–366. [CrossRef]
67. Ahern, F.J.; Erdle, T.; Maclean, D.A.; Kneppeck, I.D. A quantitative relationship between forest growth rates and thematic mapper reflectance measurements. *Int. J. Remote Sens.* **1991**, *12*, 387–400. [CrossRef]
68. R Core Team. *R: A Language and Environment for Statistical Computing v. 4.0.3*; R Foundation for Statistical Computing: Vienna, Austria, 2020.
69. Kaufman, L.; Rousseeuw, P.J. Agglomerative Nesting (Program AGNES). In *Finding Groups in Data: An Introduction to Cluster Analysis*; Wiley Series in Probability and Statistics; John Wiley & Sons, Inc.: Hoboken, NJ, USA, 1990; pp. 199–252. ISBN 978-047-173-578-6.
70. Maechler, M.; Rousseeuw, P.J.; Struyf, A.; Hubert, M.; Hornik, K. Cluster: Cluster Analysis Basics and Extensions. R package version 2.1.2. For new features, see the 'Changelog' file (in the package source). 2021. Available online: https://CRAN.R-project.org/package=cluster (accessed on 6 April 2021).
71. Fox, J.; Weisberg, S. *An R Companion to Applied Regression*, 3rd ed.; Sage: Thousand Oaks, CA, USA, 2019.
72. Mallinis, G.; Mitsopoulos, I.; Chrysafi, I. Evaluating and comparing Sentinel 2A and Landsat-8 Operational Land Imager (OLI) spectral indices for estimating fire severity in a Mediterranean pine ecosystem of Greece. *GIsci. Remote Sens.* **2018**, *55*, 1–18. [CrossRef]
73. García-Llamas, P.; Suárez-Seoane, S.; Fernández-Guisuraga, J.M.; Fernández-García, V.; Fernández-Manso, A.; Quintano, C.; Taboada, A.; Marcos, E.; Calvo, L. Evaluation and comparison of Landsat 8, Sentinel-2 and Deimos-1 remote sensing indices for assessing burn severity in Mediterranean fire-prone ecosystems. *Int. J. Appl. Earth Obs. Geoinf.* **2019**, *80*, 137–144. [CrossRef]
74. Veraverbeke, S.; Rogers, B.M.; Randerson, J.T. Daily burned area and carbon emissions from boreal fires in Alaska. *Biogeosciences* **2015**, *12*, 3579–3601. [CrossRef]
75. Hudak, A.T.; Morgan, P.; Bobbitt, M.J.; Smith, A.M.S.; Lewis, S.A.; Lentile, L.B.; Robichaud, P.R.; Clark, J.T.; McKinley, R.A. The relationship of multispectral satellite imagery to immediate fire effects. *Fire Ecol.* **2007**, *3*, 64–90. [CrossRef]
76. Kasischke, E.S.; Turetsky, M.R.; Ottmar, R.D.; French, N.H.F.; Hoy, E.E.; Kane, E.S. Evaluation of the composite burn index for assessing fire severity in Alaskan black spruce forests. *Int. J. Wildl. Fire* **2008**, *17*, 515–526. [CrossRef]
77. Giglio, L.; Boschetti, L.; Roy, D.P.; Humber, M.L.; Justice, C.O. The Collection 6 MODIS burned area mapping algorithm and product. *Remote Sens. Environ.* **2018**, *217*, 72–85. [CrossRef] [PubMed]
78. Global Forest Cover Change (GFCC) Tree Cover Multi-Year Global 30 m V003. NASA EOSDIS Land Processes DAAC. Available online: https://doi.org/10.5067/MEaSUREs/GFCC/GFCC30TC.003 (accessed on 6 April 2021).